European Journal of Medicinal Chemistry 45 (2010) 2902–2911

Contents lists available at ScienceDirect

European Journal of Medicinal Chemistry

journal homepage: http://www.elsevier.com/locate/ejmech

Original article

Diorganotin(IV) derivatives of ONO tridentate Schiff base: Synthesis, crystal structure, *in vitro* antimicrobial, anti-leishmanial and DNA binding studies

Shaukat Shujha [a], Afzal Shah [a], Zia-ur-Rehman [a], Niaz Muhammad [a], Saqib Ali [a,*], Rumana Qureshi [a], Nasir Khalid [b], Auke Meetsma [c]

[a] Department of Chemistry, Quaid-i-Azam University, Islamabad 45320, Pakistan
[b] Chemistry Division, Pakistan Institute of Nuclear Science and Technology, PO Nilore, Islamabad, Pakistan
[c] Crystal Structure Center, Chemical Physics, Zernike Institute for Advanced Materials, University of Groningen, Nijenborgh 4, NL-9747 AG Groningen, The Netherlands

ARTICLE INFO

Article history:
Received 12 August 2009
Received in revised form
11 March 2010
Accepted 15 March 2010
Available online 18 March 2010

Keywords:
N′-(2-Hydroxybenzylidene)formohydrazide
Diorganotin(IV) complexes
Crystal structure
DNA-binding

ABSTRACT

Six new diorganotin(IV) derivatives of N′-(2-hydroxybenzylidene)formohydrazide (H_2L) with general formula R_2SnL, where R = Ph (**1**), Me (**2**), Bu (**3**), Oct (**4**), *t*-Bu (**5**), Et (**6**), and L = [$OC_6H_4CHNNCHO$] have been synthesized and characterized by different analytical techniques. Crystal structure of Me_2SnL (**2**) authenticated distorted square-pyramidal geometry around the Sn atom. The CV and UV–Vis spectroscopic data indicated intercalation of complexes into DNA with binding affinity varying in the sequence: **3** (1.69×10^4 M^{-1}) > **1** (1.10×10^4 M^{-1}) > **2** (9.61×10^3 M^{-1}). Some of these compounds were found to be good antibacterial, antifungal and leishmanicidal agents.

1. Introduction

The study of organotin(IV) complexes has gained growing interest in the last four decades due to their ability to interact with DNA, indicating their potential candidature in cancer chemotherapy [1–4]. Several organotin(IV) Schiff base complexes have been investigated for their structural diversity and biocidal activities [5–7]. Cagnoli et al. found some organotin(IV) complexes to be even more active *in vitro* than the clinically used *cis*-platin [8]. Some other workers have established the quantitative structure/activity and structure/property relationships of these compounds [9]. However, little work has been carried out on the ONO donor tridentate chelating ligands, derived from the condensation of salicylaldehyde with hydrazides [10]. The present work is centered on the synthesis of diorganotin(IV) Schiff base derivatives of formic hydrazide and their characterization by different analytical techniques. Some of these compounds have good antimicrobial activities. Keeping the anticancer activity of dibutyltin(IV) complexes [11] in view, we selected three potential antitumor organotin(IV) complexes, with the one having dibutyltin(IV) moiety to evaluate their DNA binding parameters. Up to our knowledge, this is the first report on the *in vitro* evaluation of the binding parameters of organotin(IV) schiff base complexes with DNA by electrochemical and spectroscopic techniques.

2. Results and discussion

2.1. Synthesis

The ligand was synthesized by direct reaction of formic hydrazide with salicylaldehyde in ethanol. The yellow organotin(IV) complexes were prepared by reacting together ligand, organotin (IV) dichloride, triethylamine in 1:1:2 and ligand, dioctyltin(IV) oxide in 1:1 ratios in dry toluene. All the compounds were obtained in good yield. The detailed syntheses and physical data are presented in Experimental section.

2.2. Spectroscopic studies

In the ligand the vibration bands appearing at 3345, 3184 and 1689 cm^{-1} were assigned to ν_{N-H}, ν_{O-H} and $\nu_{C=O}$ vibration modes, respectively. Due to enolization and deprotonation of the ligand on complexation with diorganotin moiety, these bands disappeared. The shifting of $\nu_{C=N}$ band at 1613 cm^{-1} to lower energy suggested

* Corresponding author. Tel.: +925190642208; fax: +92512873869.
E-mail address: drsa54@yahoo.com (S. Ali).

0223-5234/$ – see front matter © 2010 Elsevier Masson SAS. All rights reserved.
doi:10.1016/j.ejmech.2010.03.015

the coordination of azomethine nitrogen with Sn atom [12]. The shifting of ν_{N-N} band from 1053 cm^{-1} to 1072–1082 cm^{-1} on complexation is attributed to the decrease in repulsion of the lone pairs of electrons on the nitrogen atoms [13]. New bands were also observed in the region of 500–555 cm^{-1} (ν_{Sn-O}) and 450–470 cm^{-1} (ν_{Sn-N}) [14].

The ^{1}H NMR spectral data showed signals at 10.12, 11.67 and 8.68 ppm due to –OH, –CHO and –NHN= protons, respectively. All these signals were absent from the spectra of complexes owing to the conversion of the aldo-imine form of ligand to imine-ol form and subsequent deprotonation. The coordination of azomethine nitrogen with Sn atom shifted the CH=N proton resonance signal down field to 8.60–8.65 ppm with ^3J (^{119}Sn, ^{1}H) coupling constant value of 38–51 Hz. All the other protons of the ligand and the R groups bonded to Sn atom appeared in the expected region. The ^2J (^{119}Sn, ^{1}H) coupling constant (79 Hz) of complex **2** corresponding to C–Sn–C angel of 129.6° was evaluated by Lockhart's equation, $\theta = 0.0161\ [^2J]^2 - 1.32\ [^2J] + 133.4$ [15]. Thus, confirmed five-coordinate Sn atom in solution. In ^{13}C NMR, the angle calculated (127.4–133.4°) for compounds **2**, **3**, **5** and **6**, using equation $^1J = 10.7\theta - 778$ [16], affirmed penta-coordination of Sn in solution. In all complexes, the signals observed in ^{13}C NMR are in conformity with expected composition.

The presence of a single ^{119}Sn peak for complexes **1**–**6** in the range −163.2 to −337 ppm is in conformity with the formation of a single species having penta-coordinated Sn atom [17].

2.3. Mass spectrometry

The ligand and its complexes showed molecular ion peak of significant intensity with the characteristic peak pattern of Sn. The proposed fragmentation pattern of ligand and complex **2** is depicted in Scheme 6. The initial fragmentation is due to the loss of a methyl group, which then gave a base peak $[C_8H_6N_2O_2Sn]^+$ in the spectrum due to the elimination of a second methyl group. The other fragments with significant abundances were $[CH_3Sn]^+$, $[CH_3Sn]^+$ and $[Sn]^+$. The rest of the diorganotin(IV) compounds followed almost the same fragmentation route as **2**, the mass spectral data is given in the Experimental section.

2.4. Crystal structure

The molecular structure with atomic numbering scheme for compound **2** is given in Fig. 1. The crystallographic data, selected bond lengths and angles are listed in the Tables 1 and 2. The

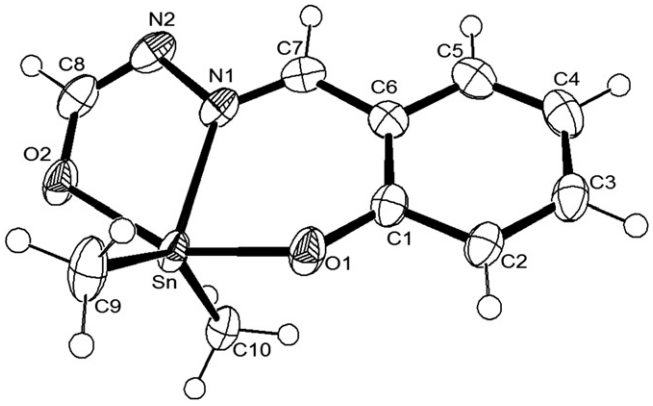

Fig. 1. ORTEP view of Me_2SnL (**2**) with atomic numbering scheme. Thermal ellipsoids are drawn at the 50% probability level. Hydrogen atoms are shown as spheres of arbitrary radii.

Table 1
Crystal data and structure refinement parameters for Me_2SnL (**2**).

Empirical formula	$C_{10}H_{12}N_2O_2Sn$
Formula mass	310.93
Crystal system	Tetragonal
Space group	$I4_1/a$, 88
a (Å)	13.4693(4)
b (Å)	13.4693(4)
c (Å)	24.9037(17)
V (Å^3)	4518.1(4)
$Z(Z')$	16(1)
Crystal habit/size (mm)	Block/0.35 × 0.29 × 0.15
T (K)	100(1)
ρ (g cm^{-3})	1.828
μ (Mo K$_\alpha$) (cm^{-1})	22.44
$F(000)$	2432
Total reflections	19718
Independent reflections	2799
For ($F_o \geq 4.0\ \sigma\ (F_o)$)	2749
$R(F) = \sum(\|\|F_o\| - \|F_c\|\|)/\sum\|F_o\|$ for $F_o > 4.0\ \sigma\ (F_o)$	0.0223
$wR(F^2) = [\sum[w(F_o^2 - F_c^2)^2]/[\sum w(F_o^2)^2]]^{1/2}$	0.0558
Goodness-of-fit	1.043
θ Range (°)	2.69–29.28
Data/restrictions/params	2799/0/139
Largest diff. peak and hole (e Å^{-3})	−0.12 and 0.17(4)

bond distances and angles of the complex **2** are comparable with the values for analogous compounds [18]. The structure of complex **2** consists of a deprotonated ONO dibasic tridentate ligand bonded to the $(CH_3)_2Sn(IV)$ moiety via two oxygen and a nitrogen atom, forming a O_2NC_2 core around the Sn atom. The ligand is non-planar, probably due to the steric requirements of the five and six membered chelate rings formed. The geometry around Sn atom can be characterized by the value of $\tau = (\beta - \alpha)/60$, where β is the largest and α the second largest basal angles around the Sn atom. The τ value is zero for perfect square pyramid ($\alpha = \beta = 180°$) and unity for a perfect trigonal pyramidal geometry ($\alpha = 120°$) [19]. For compound **2** (β = O1–Sn–O2 = 152.9° and α = C9–Sn–C10 = 140.7°) the τ value (0.2) indicates a distorted square-pyramidal geometry with two enolic oxygens and two methyl carbons in the equatorial positions and the azomethinic nitrogen at the apical position. The tendency of going from trigonal-bipyramidal geometry towards a square-pyramidal one is most probably associated with secondary intermolecular Sn···O interactions (Fig. 2). The Sn–O1 and Sn–O2 bond lengths (2.110 and 2.169 Å) are less than the sum of Van der Waals radii of Sn and O (2.8 Å). The O1–Sn–N1, and O2–Sn–N1 angles are 82.25° and 72.47°, respectively. The C9–Sn–C10 angle (140.70°) show a large deviation from the linear value (180°) and the angle calculated from $^2J(^{119}Sn-^1H)$ (129.6°) and $^1J[^{119}Sn-^{13}C]$ (133.4°) by Lockhart

Table 2
Selected bond lengths (Å) and angles (°) for Me_2SnL (**2**).

Sn–O1	2.110(2)	O1–C1	1.312(4)
Sn–O2	2.169(2)	O2–C8	1.302(4)
Sn–N1	2.184(2)	N1–N2	1.409(3)
Sn–C9	2.106(4)	N1–C7	1.295(4)
Sn–C10	2.112(4)	N2–C8	1.289(4)
O1–Sn–O2	152.89(9)	N2–N1–C7	115.6(2)
O1–Sn–N1	82.25(9)	N1–N2–C8	110.0(3)
O1–Sn–C9	88.93(13)	O1–C1–C2	119.0(3)
O1–Sn–C10	96.55(10)	O1–C1–C6	123.2(2)
O2–Sn–N1	72.47(9)	Sn–O1–C1	129.21(18)
O2–Sn–C9	93.36(13)	Sn–O2–C8	113.12(18)
O2–Sn–C10	98.63(10)	Sn–N1–N2	116.97(18)
N1–Sn–C9	115.96(13)	Sn–N1–C7	127.13(19)
N1–Sn–C10	103.34(11)	N1–C7–C6	126.2(3)
C9–Sn–C10	140.70(14)	O2–C8–N2	127.1(3)

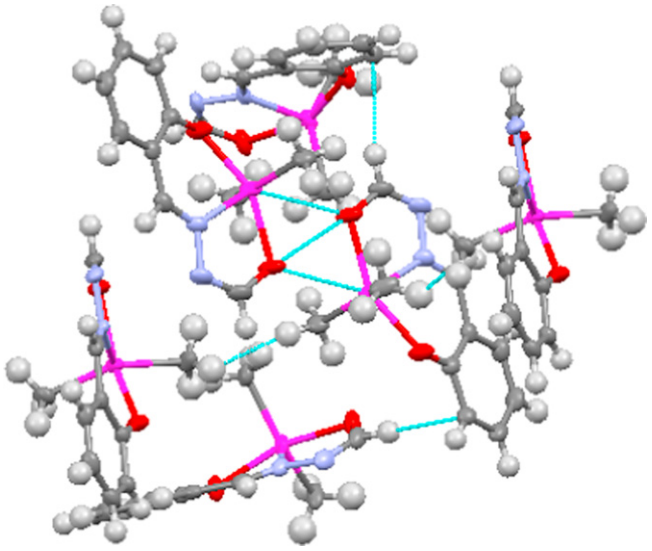

Fig. 2. The molecular packing of Me_2SnL (**2**) showing the arrangement of monomeric units.

equation [14,15]. The Sn–N1 bond distance is 2.184 Å, closer to the sum of covalent radii of Sn and N (2.15 Å) and significantly less than the sum of van der waals radii (3.75 Å). The C1–O1, C8–O2 bond length (1.313 Å, 1.302 Å) and C1–N1–N2 angle (109.99°) for compound **2** are match-well with the reported values [17].

2.5. Biological activity

2.5.1. Antibacterial activity

The Schiff base ligand and its diorganotin(IV) derivatives were screened for their antibacterial activity against 2 gram positive (*Bacillus subtilis*, *Staphylococcus aureus*) and 4 gram negative bacteria (*Eschericha coli*, *Shigella flexenari*, *Pseudomonas aeruginosa*, *Salmonella typhi*), Table 3. Despite the reported antibacterial activity of various Schiff bases [20,21], the synthesized ligand was found inactive against all bacterial strains. Most of the diorganotin (IV) derivatives significantly inhibit gram-positive bacteria growth. This may be due to the ease of permeation of the complexes owing to the simplicity in the cell wall of these strains [22]. The dimethyl- (**2**) and dibutyltin(IV)-(**3**) complexes show highest activity, which subsides as the alkyl chain length increases [23,24].

Table 3
Antibacterial activity[a–d] (diameter of inhibition zone) of *N′*-(2-hydroxylbenzylidene) formohydrazide and its diorganotin(IV) derivatives.

Bacterium (ATCC No.)	Inhibition zone diameter (mm)							Reference drug
	H_2L	1	2	3	4	5	6	
Bacillus subtillis (11774)	–	18	15	20	10	–	12	37
Staphylococcus aureus (25923)	–	–	20	15	–	10	9	26
Eschericha coli (11229)	–	15	10	18	11	12	9	30
Shigella flexenari (10782)	–	–	17	14	11	9	10	36
Pseudomonas aeruginosa (10145)	–	10	12	9	–	–	11	32
Salmonella typhi (10749)	–	–	–	17	–	15		30

[a] *In vitro* agar well-diffusion method, conc. 1 mg mL^{-1} DMSO.
[b] Reference drug, Imipenum 10 μg/disc.
[c] Zone diameter (Activity): 3–6 mm (non significant), 7–9 mm (low), 10–12 mm (good), >12 mm (significant).
[d] Clinical Implication: *Escherichia coli*, infection of wounds, urinary tract and dysentery; *Bacillus subtilis*, food poisoning; *Shigella flexenari*, blood diarrhea with fever and severe prostration; *Staphylococcus aureus*, food poisoning, scaled skin syndrome, endocarditis; *Pseudomonas aeruginosa*, infection of wounds, eyes, septicemia, *Salmonella typhi*, typhoid fever, localized infection [25].

2.5.2. Antifungal activity

The antifungal activity of synthesized compounds were tested *in vitro* against human pathogenic fungal strains including yeasts (*Candida albicans* ATCC 2192, *Candida glabrata* ATCC 90030), dermatophytes (*Microsporum canis* ATCC 9865, *Trichphyton longifusus* ATCC 22397), opportunistic moulds (*Aspergillus flavus* ATCC 1030 and *Fusarium solani* ATCC 11712) by using the agar tube dilution test. Micoanazole (200 μg/ml) and Amphotericin B (200 μg/ml) were used as standards drugs. The percent growth inhibition of the compounds is summarized in Table 4. All the fungal strains except *A. flavus* are resistant to the ligand. Activity of compounds **1**, **2** and **6** is fairly good while for the rest of the compounds low activity was observed.

2.5.3. Cytotoxicity

The *in vivo* lethality to *brine shrimp nauplii* was used to assess the cytotoxicity of synthesized compounds [25]. The results are presented in Table 5. Compound **3** show highest toxicity larger than the standard drug with LD_{50} 0.691 μg/ml.

2.5.4. Anti-leishmanial activity

The Anti-leishmanial activity of ligand and complexes (**1**–**6**) were obtained against the pathogenic Leishmania major, using Amphotericin B (0.50 μg/ml) and Pentamidine (5.78 μg/ml) as standard drugs. The data are presented in Table 6. The reported compounds produced a significant reduction in viable promastigotes. Compound **6** has the highest potential as leishmanicidal agent with IC_{50} 0.90 μg/ml followed by compound **3** (IC_{50} 0.96 μg/ml) and **5** (IC_{50} 0.98 μg/ml). The activity of these compounds is excellent and far exceed the level for the reported organotin(IV) compounds [26].

2.6. Voltammetric study of complex-DNA interaction

The cyclic voltammetric behavior of 3.00 mM complex **1** in the absence and presence of 50 μM DNA at bare GCE is shown in Fig. 3A. The voltammogram of the free complex **1** shown in Fig. 3A(a) featured a single well defined and stable cathodic peak at −1.531 V versus SCE in 10% aqueous DMSO at 25 °C. The absence of anodic peak in the reverse scan indicated the irreversibility of the electrochemical process. The electrochemical signal at −1.531 V is attributed to the reduction of Sn^{+4} to Sn^{+2} state. The broadness of the peak as indicated by $|E_p - E_{p/2}| = 70$ mV, may be due to the overlap of two $1e^-$ reduction peaks. The cyclic voltammogram of complex **1** in the presence of 50 μM DNA (Fig. 3A(b)), underwent

Table 4
Antifungal activity [a,b,c] (% inhibition) of *N′*-(2-hydroxybenzylidene)formohydrazide and its diorganotin(IV) derivatives.

Fungus (ATCC No.)	Inhibition %							MIC (μg/ml)
	H_2L	1	2	3	4	5	6	
Candida albicans (2129)	0	0	35	0	30	10	20	110.8
Aspergeilus flavus (1030)	40	50	45	10	0	0	40	20.0
Microsporum canis (9865)	0	10	0	0	10	20	0	98.4
Fusarium solani (11712)	0	0	40	20	0	0	30	73.2
Trichophyton longifusus (22397)	0	40	20	0	0	0	0	70.0
Candida glabrata (90 030)	0	50	0	0	5	0	35	110.8

[a] Concentration: 200 μg mL^{-1} of DMSO.
[b] MIC: Minimum inhibitory concentration.
[c] % (standard drug) = 100.

Table 5
Brine Shrimp (*Artemia salina*) lethality bioassay of *N′*-(2-ydroxybenzylidene) formohydrazide and its diorganotin(IV) complexes.

Sample Code	H_2L	1	2	3	4	5	6
LD_{50} μg/ml	–	–	95.70	0.691	–	–	88.30

Standard drug Etoppside LD_{50} 7.46 μg/mL.

31.46% decrease in peak current and 79 mV positive shift in peak potential. The substantial diminution in peak current can presumably be due to the decrease in free drug concentration due to the formation of slowly diffusing, heavy molecular weight **1**-DNA adduct. The obvious positive peak potential shift could be attributed to the intercalation of **1** into the stacked base pair pockets of DNA as reported by the previous investigators [27,28]. The voltammetric parameters obtained from the cyclic voltammograms of 3.00 mM **2** and **3** with and without DNA (Fig. 3B and C) are listed in Table 7.

The greater decrease in peak current (33.65%) of **3** as compared to **2** (24.88%) by the addition of 50 μM DNA is due to the lower diffusion coefficient of **3**–DNA complex as compared to **2**–DNA, which will be discussed thoroughly in subsequent section. The positive shift in peak potentials of both the compounds by the addition of DNA reflects intercalation as the dominant mode of interaction, in which the drug inserts itself into the stacked base pairs domain of DNA.

The gradual decay in peak current of **1**, **2** and **3** by the addition of varying concentration of DNA, ranging from 10 to 60 μM, can be used to quantify the binding constants of **1**-DNA, **2**-DNA and **3**-DNA adducts by the application of the following equation [29].

$$\log(1/[\mathrm{DNA}]) = \log K + \log(I_{H-G}/(I_G - I_{H-G})) \quad (1)$$

where, K is the binding constant, I_G and I_{H-G} are the peak currents of the free guest (G) and the adduct (H – G), respectively.

The plots of log (1/[DNA]) versus log $(I_{H-G}/(I_G - I_{H-G}))$ (Fig. 4) yielded $K = 1.10 \times 10^4\ M^{-1}$, $9.61 \times 10^3\ M^{-1}$ and $1.69 \times 10^4\ M^{-1}$ for **1**-DNA, **2**-DNA and **3**-DNA complexes, respectively. The greater K value of **1** as compared to **2** is attributed to the presence of extended aromatic system which may bind strongly with DNA bases [30]. The strong affinity of **3** for DNA, indicated by its greater intercept (Fig. 4) as compared to **1** could be assigned to the additional hydrophobic interactions of the bulky butyl moiety with the nucleotide bases. The K values of these diorganotin(IV) – DNA adducts are greater than those observed for similar DNA-intercalating Cr and Ru complexes, $[CrCl_2(dicnq)_2]^+$ and $[Ru(dicnq)_3]^{+2}$, for which the binding constants have been reported as 1.20×10^3 and $9.70 \times 10^3\ M^{-1}$, respectively [31–33].

To know whether the electrochemical process is diffusion controlled or adsorption controlled, the values of peak current, I were plotted vs. the square root of the scan rate ($\nu^{1/2}$) in the presence and absence of DNA using Randles–Sevcik equation for irreversible process [34,35].

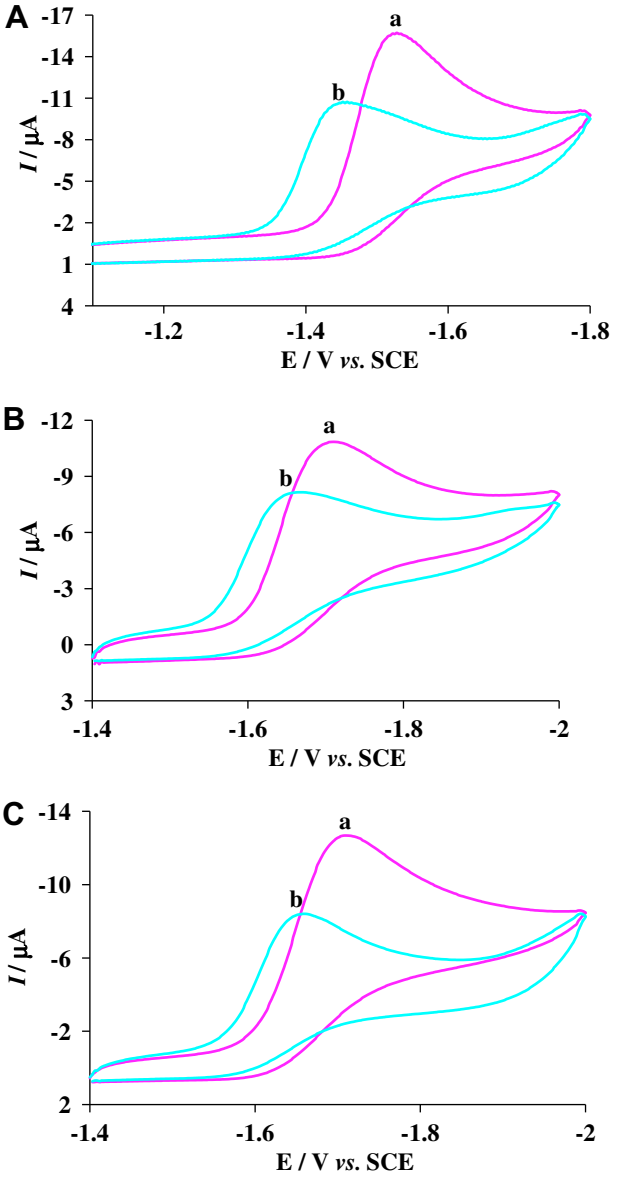

Fig. 3. A. Cyclic voltammograms of 3.00 mM Ph_2SnL (**1**) in 10% aqueous DMSO with 0.1 M TBAP as supporting electrolyte in the absence (a) and presence of 50 μM DNA (b) at 25 °C. Working electrode: Glassy carbon with a geometric area of 0.071 cm^2, scan rate 100 mV/s. B. Cyclic voltammograms of 3.00 mM Me_2SnL (**2**) in 10% aqueous DMSO with 0.1 M TBAP as supporting electrolyte in the absence (a) and presence of 50 μM DNA (b) at 25 °C. Working electrode: Glassy carbon with a geometric area of 0.071 cm^2, scan rate 100 mV/s. C. Cyclic voltammograms of 3.00 mM Bu_2SnL (**3**) in 10% aqueous DMSO with 0.1 M TBAP as supporting electrolyte in the absence (a) and presence of 50 μM DNA (b) at 25 °C. Working electrode: Glassy carbon with a geometric area of 0.071 cm^2, scan rate 100 mV/s.

Table 6
Anti-leishmanial activity of *N′*-(2-hydroxybenzylidene)formohydrazide and its diorganotin(IV) complexes.

Sample Code	IC_{50} (μg/ml) ± S.D
H_2L	24.0 ± 0.02
1	6.50 ± 0.04
2	2.08 ± 0.04
3	0.96 ± 0.02
4	4.26 ± 0.04
5	0.98 ± 0.02
6	0.90 ± 0.02

$$I = 2.69 \times 10^5 n(\alpha n)^{1/2} A C_o^* D^{1/2} \nu^{1/2} \quad (2)$$

Where I is the peak current (A), A is the surface area of the electrode (cm^2), C_o^* is the bulk concentration (mol cm^{-3}) of the electroactive species, D is the diffusion coefficient ($cm^2\ s^{-1}$), α is the transfer coefficient with a value of 0.34 as obtained from $|E_p - E_{p/2}| = 47.7\ mV/\alpha n$ and ν is the scan rate ($V\ s^{-1}$).

The linearity of the plots demonstrates that the main mass transport of these complexes (Fig. 4A) and their DNA adducts (Fig. 4B), to the electrode surface is controlled by diffusion step [36]. The diffusion coefficients of the free and DNA bound adducts of

Table 7
Voltammetric parameters of compound **1**–**3** in the absence and presence of DNA.

Substance	ν/V s^{-1}	[DNA]/μM	I/μA	E_{pc}/V	Shift in E_{pc}/m V	% Decrease in I
1	0.1	0	−15.63	−1.531	79	31.46
1-DNA	0.1	50	−10.71	−1.452		
2	0.1	0	−10.85	−1.710	46	24.88
2-DNA	0.1	50	−8.15	−1.664		
3	0.1	0	−12.67	−1.713	52	33.65
3-DNA	0.1	50	−8.41	−1.661		

diorganotin(IV) complexes (Table 8) were determined from the slopes of Randles–Sevcik plots. The lower diffusion coefficients of the DNA bound species are responsible for the decay of peak currents in cyclic voltammograms shown in Fig. 3.

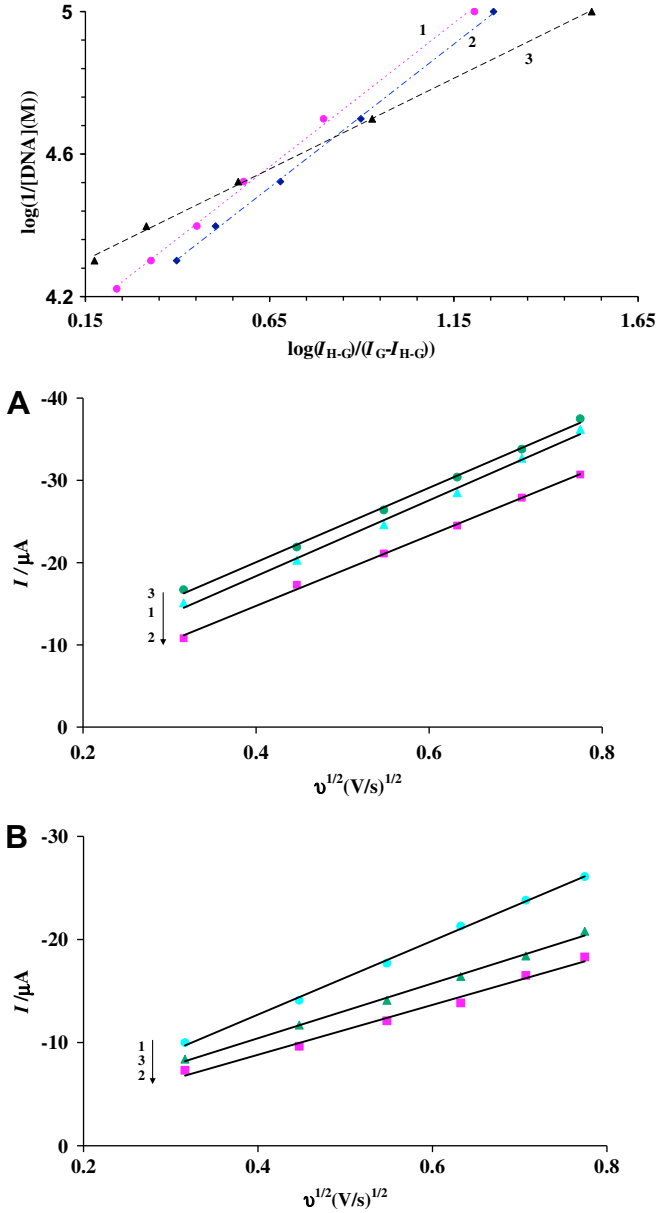

Fig. 4. Plots of log ($I_{H-G}/(I_G - I_{H-G})$) vs. log (1/[DNA]) used to calculate the binding constants of **1**-DNA, **2**-DNA and **3**-DNA adducts. A. Plots of I vs. $\nu^{1/2}$, for the determination of diffusion coefficients of the free drugs (3.00 mM **1**–**3**). Scan rates 0.1–0.6 V/s with a difference of 0.1 V/s. B. Plots of I vs. $\nu^{1/2}$, for the determination of the diffusion coefficients of the DNA bound drugs by taking 3.00 mM **1**–**3** and 60 μM DNA. Scan rate 0.1–0.6 V/s with a difference of 0.1 V/s.

2.7. UV–Vis absorption study of complex-DNA interaction

The interaction of diorganotin(IV) complexes with DNA was also examined by UV–Vis spectroscopy for getting some further clues about the mode of interaction and binding strength. The effect of varying concentration of DNA (5–25 μM) on the electronic absorption spectra of 0.2 mM of **1**, **2** and **3** is shown in Fig. 5A–C. The strong absorption of these compounds in the near UV region (292–330 nm) is attributed to the long-living triplet excited state of the aromatic system. The underlying principle behind the broad absorption bands in the region (350–470 nm) is the transition between π–π* and n–π* energy levels of the tridentate ligand *N′*-(2-hydroxybenzylidene)formohydrazide. The absorption spectra of **1**, **2** and **3** recorded a 68.26, 62.83 and 65.91% decrease in peak intensities accompanied with 2, 5 and 3 nm red shift, by the addition of 25 μM DNA. The peculiar hypochromic effects can be associated with the interaction of electronic states of the intercalating chromophore and those of the stacked base pairs of DNA [37,38]. The slight bathochromic shifts can best be described by the lowering in π–π* and n–π* transition energy of the ligands in diorganotin(IV) complexes due to their ordered stacking between the DNA base pairs after intercalation.

Based upon the decrease in absorbance, the binding constants were calculated according to the following equation [39,40].

$$\frac{A_0}{A - A_0} = \frac{\varepsilon_G}{\varepsilon_{H-G} - \varepsilon_G} + \frac{\varepsilon_G}{\varepsilon_{H-G} - \varepsilon_G} \frac{1}{K[\mathrm{DNA}]} \quad (3)$$

Where K is the binding constant, A_0 and A are absorbances of the free and DNA bound diorganotin(IV) complexes while ε_G and ε_{H-G} are their absorption coefficients respectively.

The binding constants, with values of 1.54×10^4, 8.19×10^3 and 2.59×10^4 M^{-1} for the interaction of **1**, **2** and **3** with DNA were obtained from the slope to intercept ratio of the plots (Fig. 6) between $A_0/(A - A_0)$ vs. 1/[DNA]. The results tabulated in Table 8, indicate a very close agreement in the values obtained from CV and UV–Vis spectroscopy. An examination of Table 8 reflects that the interaction of these drugs with DNA is a spontaneous process as attested by the negative values of ΔG.

3. Conclusions

Spectroscopic data and X-ray single crystal study confirmed tridentate coordination of ligand with diorganotin moiety. Due to the presence of intermolecular Sn···O interactions in compound **2**, the structure has a tendency towards a square-pyramidal geometry. The dibutyltin(IV) derivative exhibited significant inhibitory effects on gram positive bacterial strains, leshminia major and brine shrimp larvae. The results of CV and UV–Vis. spectroscopy revealed intercalative mode of interaction of these complexes with DNA as the dominant mode. The negative values of standard Gibbs energy changes ($\Delta G = -RT\ln K$) indicated the spontaneity of these interactions. This study is expected to throw light in understanding the molecular mechanism of the drug action and designing of DNA targeted drugs.

4. Experimental

4.1. Materials and methods

All reagents of analytical grade were obtained from Aldrich chemicals (USA). Tetrabutylammonium perchlorate (TBAP, Fluka, 99% purity) was further purified by recrystallization using methanol as a solvent. DMSO, ethanol and toluene were procured from E. Merck (Germany). Toulene was dried before use with standard

Table 8
The binding constants and Gibbs free energies of **1**-DNA, **2**-DNA and **3**-DNA adducts as determined by voltammetry and UV–Vis. spectroscopy along with the diffusion coefficients of the free and DNA bound species.

Drug-DNA adduct	CV				Spectroscopy	
	$10^7 D_f$/cm^2 s^{-1}	$10^8 D_b$/cm^2 s^{-1}	K/M^{-1}	$-\Delta G$/kJ mol^{-1}	K/M^{-1}	$-\Delta G$/kJ mol^{-1}
1-DNA	2.37	0.15	1.10×10^4	23.05	1.54×10^4	23.39
2-DNA	2.05	6.49	9.61×10^3	22.72	8.19×10^3	22.33
3-DNA	2.29	7.89	1.69×10^4	24.11	2.59×10^4	25.18

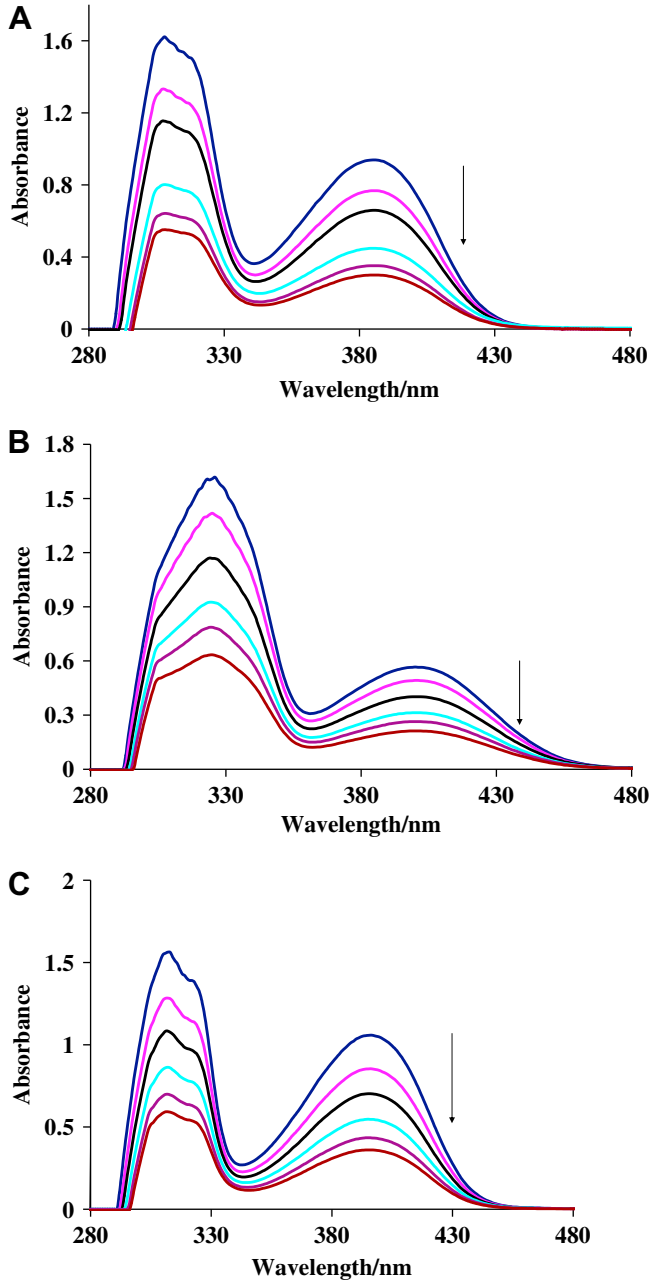

Fig. 5. A Absorption spectra of 0.2 mM Ph_2SnL (**1**) in the absence (a) and presence of 5 μM, (b) 10 μM, (c) 15 μM, (d) 20 μM, (e), and 25 μM DNA (f). The arrow direction indicates increasing concentrations of DNA. B. Absorption spectra of 0.2 mM Me_2SnL (**2**) in the absence (a) and presence of 5 μM, (b) 10 μM, (c) 15 μM, (d) 20 μM, (e), and 25 μM DNA (f). The arrow direction indicates increasing concentrations of DNA. C. Absorption spectra of 0.2 mM Bu_2SnL (**3**) in the absence (a) and presence of 5 μM, (b) 10 μM, (c) 15 μM, (d) 20 μM, (e), and 25 μM DNA (f). The arrow direction indicates increasing concentrations of DNA.

procedure [41]. The melting points were determined on an electrothermal melting point apparatus, model MP-D Mitamura Riken Kogyo (Japan) by using capillary tubes and are uncorrected. Elemental analyses were performed using Leco CHNS-932 elemental analyzer (USA). The IR spectra of all samples were recorded as KBr discs or in NaCl cells using Bio-Rad Excaliber FT-IR, model FTS 300 MX spectrometer (USA) in range of 4000–400 cm^{-1}. NMR (^{1}H and ^{13}C) spectra were obtained on a Brucker 300 MHz FT NMR spectrometer using $CDCl_3$ as solvent. ^{119}Sn NMR spectra were obtained with Me_4Sn as an external reference. The cyclic voltammetric experiments were performed by PGSTAT 302 with Autolab GPES version 4.9 Eco Chemie, Utrecht, the Netherlands. Measurements were carried out in a conventional three electrode cell with saturated calomel electrode (SCE) from Fisher scientific company (Cat No. 13-639-51) as a reference electrode, a thin Pt wire of thickness 0.5 mm with an exposed end of 10 mm as the counter electrode and a bare glassy carbon electrode (GCE) with a geometric area of 0.071 cm^2 as the working electrode. Prior to experiments, the GCE was polished with 0.25 μm diamond paste on a nylon buffing pad. For electrochemical measurements the test solution was kept in an electrochemical cell (model K64 PARC) connected to the circulating thermostat LAUDA model K-4R. Argon was used for flushing out oxygen before every electrochemical assay. Absorption spectra were measured on a UV–Vis Spectrometer; Shimadzu 1601. Table Top Centrifuge, Model PLC-05 (Taiwan) was used for the extraction of DNA.

4.2. Synthesis

4.2.1. Synthesis of Schiff base ligand

An ethanolic solution of salicylaldehyde (0.1 mol, 12.2 g) was added slowly to the solution of formic hydrazide (0.1 mol, 6.0 g) in ethanol with constant stirring. The mixture was refluxed for 1 h and on cooling crystalline solid product was obtained (Scheme 1). The structure of ligand and numbering scheme are given in Scheme 2.

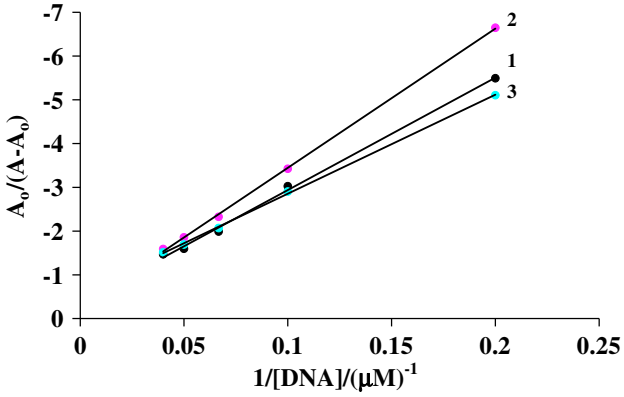

Fig. 6. Plots of $A_o/(A - A_o)$ vs. 1/[DNA] for the determination of binding constants of Complex-DNA adducts by taking 0.2 mM drug and 5–25 μM DNA with a difference of 5 μM aliquot of DNA.

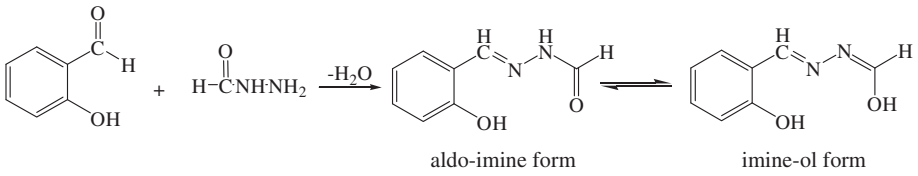

Scheme 1. Synthesis of ligand (H_2L).

4.2.1.1. 2.2.1.1.N′-(2-hydroxybenzylidene)formohydrazide. Yield 82%, m.p. 187–189 °C. Anal. Calc. for $C_8H_8N_2O_2$ (M = 164): C, 58.53; H, 4.91; N, 17.06. Found: C, 58.49; H, 4.89; N, 17.03%. EI-MS, m/z (%): $[C_8H_8N_2O_2]^+$ 164 (50), $[C_7H_7N_2O]^+$ 135 (8), $[C_7H_6NO]^+$ 120 (80), $[C_7H_5NO]^+$ 119 (100), $[C_7H_7O]^+$ 107 (11), $[C_6H_5]^+$ 77 (44), $[C_5H_5]^+$ 65 (24), $[C_4H_9]^+$ 57 (3), $[C_4H_3]^+$ 51 (38) FT-IR (cm^{-1}, KBr): 3355m, ν_{N-H}; 3184m, ν_{O-H}; 1701s, $\nu_{C=O}$; 1613m, $\nu_{C=N}$; 1053m, ν_{N-N}. ^{1}H NMR (ppm): H-2: 6.89 (d, 1H, phenyl, $^3J_{H-H}$ = 8.4), H-3: 7.24 (t, 1H, phenyl, $^3J_{H-H}$ = 7.6), H-4: 6.85 (t, 1H, phenyl, $^3J_{H-H}$ = 7.8), H-5: 7.60 (d, 1H, phenyl, $^3J_{H-H}$ = 7.6), H-7: 8.32 (s, 1H, CH=N), H-8: 11.67 (s, 1H, CHO), NH: 8.68 (s, 1H, NH), OH: 10.12 (s, 1H, OH), ^{13}C NMR (ppm): C-7: 148.1 (HC=N); C-8: 165.2 (CHONH); 157.4, 116.8, 132.3, 120.1, 131.6, 119.1 (Ph-C)

*4.2.2. Synthesis of the complexes (**1**–**6**)*

The diorganotin(IV) complexes were synthesized by two method.

Method I: A 3.0 mmol (0.49 g) of *N′*-(2-hydroxybenzylidene) formohydrazide, 6 mmol (0.83 ml) triethylamine and dialkylltin dichloride (3.0 mmol) were mixed together in 100 ml toluene. After 5 h stirring at room temperature, the yellow solution was filtered off to remove the Et_3NHCl salt. The filtrate was rotary evaporator to get a yellow product (Scheme 3).

Method II: The dioctyltin(IV) complex was synthesized by suspending the dioctyltin(IV) oxide and ligand in stoichiometric amounts in dry toluene. The mixture was refluxed for 3 h, and water formed during the reaction was removed by the Dean and Stark apparatus. Yellow oily product was obtained by removing solvent under reduce pressure (Scheme 4).

The structure and numbering template of diorganotin(IV) complexes is illustrated in Scheme 5.

*4.2.2.1. Diphenyltin(IV) [N-(2-oxidobenzylidene)-N′-(oxidomethylene) hydrazine] (**1**).* Yield 84%, m.p. 160–162 °C. Anal. Calc. for $C_{20}H_{16}N_2O_2Sn$ (M = 436): C, 55.21; H, 3.71; N, 6.44. Found: C, 55.19; H, 3.72; N, 6.39%. EI-MS, m/z (%): $[C_{20}H_{16}N_2O_2Sn]^+$ 436 (56), $[C_{14}H_{11}N_2O_2Sn]^+$ 359 (22), $[C_8H_6N_2O_2Sn]^+$ 282 (100), $[C_8H_8N_2O_2]^+$ 165 (11), $[C_7H_9N_2O]^+$ 137 (11), $[C_7H_6NO]^+$/$[Sn]^+$ 120 (37), $[C_7H_5NO]^+$ 119 (11), $[C_6H_5]^+$ 77 (36), $[C_4H_9]^+$ 57 (5) $[C_4H_3]^+$ 51 (27), $[C_6H_5Sn]^+$ 197 (48) FT-IR (cm^{-1}, KBr): 1609s, $\nu_{C=N}$; 567m, ν_{Sn-O}; 1074m, ν_{N-N}; 486w, ν_{Sn-N}. ^{1}H NMR (ppm): H-2: 7.12 (d, ^{1}H, phenyl, $^3J_{H-H}$ = 8.4), H-3: 7.41–7.50 (m, 1H, phenyl), H-4: 6.81 (t, 1H, phenyl, $^3J_{H-H}$ = 7.8), H-5: 7.21 (d, 1H, phenyl, $^3J_{H-H}$ = 7.8), H-7: 8.65 [(s, 1H, CH=N), $^3J(^{119}Sn-^1H)$ = 51 Hz], H-8: 7.38–7.51 (m, 1H, N=CH), H-β: 7.84–7.90 (m, 4H, phenyl), H-γ, H-δ: 7.38–7.51 (m, 6H, phenyl), ^{13}C NMR (ppm): C-7: 163.0 (HC=N), C-8: 167.5 (CO=N), 163.6, 135.8, 134.7, 122.2, 11.7, 116.3 (Ph-C); C-α: 139.0, C-β: 136.7 ^2J [^{119}Sn–^{13}C] = 56 Hz, C-γ: 129.0 $^3J[^{119/117}Sn-^{13}C]$ = 97, 89 Hz, C-δ: 130.7 $^4J[^{119}Sn-^{13}C]$ = 17 Hz, ^{119}Sn NMR: δ = −337 Hz

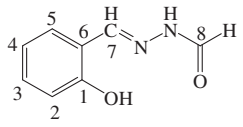

Scheme 2. Numbering scheme of ligand (H_2L).

*4.2.2.2. Dimethyltin(IV) [N-(2-oxidobenzylidene)-N′-(oxidomethylene) hydrazine] (**2**).* Yield 80%, m.p. 116–118 °C. Anal. Calc. for $C_{10}H_{12}N_2O_2Sn$ (M = 312): C, 38.63; H, 3.89; N, 9.01. Found: C, 38.59; H, 3.85; N, 9.03%. EI-MS, m/z (%): $[C_{10}H_{12}N_2O_2Sn]^+$ 312 (84), $[C_9H_9N_2O_2Sn]^+$ 297 (80), $[C_8H_6N_2O_2Sn]^+$ 282 (100), $[C_8H_8N_2O_2]^+$ 164 (6), $[C_7H_9N_2O]^+$ 137 (27), $[C_7H_6NO]^+$/$[Sn]^+$ 120 (51), $[C_7H_5NO]^+$ 119 (23), $[C_6H_5]^+$ 77 (23), $[C_4H_3]^+$ 51 (48), $[C_2H_6Sn]^+$ 150 (5), $[CH_3Sn]^+$ 135 (71) FT-IR (cm^{-1},KBr): 1605s, $\nu_{C=N}$; 563m, ν_{Sn-O}; 1072m, ν_{N-N}, 484w,ν_{Sn-N}.

^{1}H NMR (ppm): H-2: 6.77 (d, 1H, phenyl, $^3J_{H-H}$ = 8.1), H-3: 7.36 (t, 1H, phenyl, $^3J_{H-H}$ = 7.8), H-4: 6.75 (t, 1H, phenyl, $^3J_{H-H}$ = 7.8), H-5: 7.18 (d, 1H, phenyl, $^3J_{H-H}$ = 7.8), H-7: 8.62 [(s, 1H, CH=N), $^3J(^{119}Sn-^1H)$ = 46 Hz], H-8: 7.63 (s, 1H, N=OCH), H-α: 0.83 (s, 6H, $2CH_3$), $^2J(^{119/117}Sn-^1H)$ = 79, 76 Hz ^{13}C NMR (ppm): C-7: 162.8 (HC=N), C-8: 166.6 (CO=N), 163.7, 135.8, 134.5, 121.8, 117.3, 116.2 (Ph-C), $C_α$: 1.55 $^1J[^{119/117}Sn-^{13}C]$ = 650, 620 Hz, ^{119}Sn NMR: δ = −163 Hz

*4.2.2.3. Dibutyltin(IV) [N-(2-oxidobenzylidene)-N′-(oxidomethylene) hydrazine] (**3**).* Yield 78%, m.p. viscous liquid. Anal. Calc. for $C_{16}H_{24}N_2O_2Sn$ (M = 396): C, 48.64; H, 6.12; N, 7.09. Found: C, 48.61; H, 6.10; N, 7.06%. EI-MS, m/z (%): $[C_{16}H_{24}N_2O_2Sn]^+$ 396 (32), $[C_{12}H_{15}N_2O_2Sn]^+$ 339 (76), $[C_8H_6N_2O_2Sn]^+$ 282 (100), $[C_8H_8N_2O_2]^+$ 164 (21), $[C_7H_9N_2O]^+$ 137 (26), $[C_7H_6NO]^+$/$[Sn]^+$ 120 (26), $[C_7H_5NO]^+$ 119 (16), $[C_4H_9]^+$ 57 (99), $[C_4H_3]^+$ 51 (6), $[C_8H_{18}Sn]^+$ 234 (12). FT-IR (cm^{-1}, KBr): 1609s, $\nu_{C=N}$; 565m, ν_{Sn-O}; 1080m, ν_{N-N}; 481w, ν_{Sn-N}, ^{1}H NMR (ppm): H-2: 6.77 (d, 1H, phenyl, $^3J_{H-H}$ = 8.1), H-3: 7.35 (t, 1H, phenyl, $^3J_{H-H}$ = 7.8), H-4: 6.73 (t, 1H, phenyl, $^3J_{H-H}$ = 7.8), H-5: 7.16 (d, 1H, phenyl, $^3J_{H-H}$ = 7.8), H-7: 8.61 [(s, 1H, CH=N), $^3J(^{119}Sn-^1H)$ = 43 Hz], H-8: 7.66 (s, 1H, N=OCH), H-α: 1.60–1.69 (m, 4H, $2CH_2$), H-β: 1.48–1.54 (m, 4H, $2CH_2$), H-γ: 1.36 (m, 4H, $2CH_2$), H-δ: 0.89 (t, 6H, $2CH_3$, $^3J_{H-H}$ = 7.2), ^{13}C NMR (ppm): C-7: 162.7 (HC=N), C-8: 167.2 (CO=N), 164.0, 135.6, 134.5, 121.7, 117.0, 116.2 (Ph-C), C-α: 22.4 $^1J[^{119/117}Sn-^{13}C]$ = 600, 575 Hz, C-β: 26.8 $^2J[^{119}Sn-^{13}C]$ = 36 Hz, C-γ: 26.2 $^3J[^{119}Sn-^{13}C]$ = 90 Hz, C-δ: 13.6 (Sn–Bu). ^{119}Sn NMR: δ = −202 Hz

*4.2.2.4. Dioctyltin(IV) [N-(2-oxidobenzylidene)-N′-(oxidomethylene) hydrazine] (**4**).* Yield 77%, m.p. Viscous liquid. Anal. Calc. for $C_{24}H_{40}N_2O_2Sn$ (M = 508): C, 56.82; H, 7.95; N, 5.52. Found: C, 56.79; H, 7.92; N, 5.49%. EI-MS, m/z (%): $[C_{24}H_{40}N_2O_2Sn]^+$ 508 (4), $[C_{16}H_{23}N_2O_2Sn]^+$ 395 (14), $[C_8H_7N_2O_2Sn]^+$ 283 (64), $[C_8H_6N_2O_2Sn]^+$ 282 (32), $[C_8H_8N_2O_2]^+$ 164 (10), $[C_7H_9N_2O]^+$ 137 (13), $[C_7H_6NO]^+$/$[Sn]^+$ 120 (9), $[C_7H_5NO]^+$ 119 (7), $[C_6H_5]^+$ 77 (4), $[C_4H_9]^+$ 57 (100), $[C_4H_3]^+$ 51 (4). FT-IR (cm^{-1}, KBr): 1603s, $\nu_{C=N}$; 566m, ν_{Sn-O}; 1082m, ν_{N-N}; 489w, ν_{Sn-N}, ^{1}H NMR (ppm): H-2: 6.76 (d, 1H, phenyl, $^3J_{H-H}$ = 8.1), H-3: 7.35 (t, 1H, phenyl, $^3J_{H-H}$ = 7.8), H-4: 6.70 (t, 1H, phenyl, $^3J_{H-H}$ = 7.8), H-5: 7.16 (d, 1H, phenyl, $^3J_{H-H}$ = 7.8), H-7: 8.61 [(s, 1H, CH=N), $^3J(^{119}Sn-^1H)$ = 41 Hz], H-8: 7.66 (s, 1H, N=OCH), H-α: 1.65–1.72 (m, 4H, $2CH_2$), H-β: 1.49–1.58 (m, 4H, $2CH_2$), H-γ-γ′: 1.23–1.46 (br, 16H, $2CH_2$ CH_2CH_2 CH_2), H-δ′: 0.88 (t, 6H, $2CH_3$, $^3J_{H-H}$ = 7.2), ^{13}C NMR (ppm): C-7: 162.6 (HC=N), C-8: 167.2

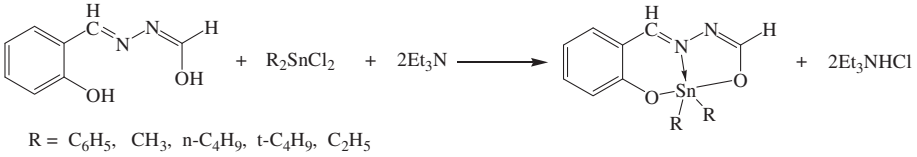

Scheme 3. Synthesis of diorganotin(IV) derivatives (**1**–**5**).

(CO═N), 164.0, 135.6, 134.5, 121.8, 117.0, 116.2 (Ph-C); C-α: 22.1, C-β: 24.65, $^{2}J[^{119}Sn-^{13}C] = 36$ Hz, C-γ: 33.4, $^{3}J[^{119}Sn-^{13}C] = 82$ Hz, C-δ: 29.2, C-α′: 29.1, C-β′: 31.8, C-γ′: 22.7, C-δ′: 14.1. ^{119}Sn NMR: $\delta = -180$ Hz

*4.2.2.5. Di-ter-butyltin(IV) [N-(2-oxidobenzylidene)-N′-(oxidomethylene)hydrazine] (**5**).* Yield 78%, m.p. Viscous liquid. Anal. Calc. for $C_{16}H_{24}N_2O_2Sn$ ($M = 396$): C, 48.64; H, 6.12; N, 7.09. Found: C, 48.59; H, 6.09; N, 7.12%. EI-MS, *m/z* (%): $[C_{16}H_{24}N_2O_2Sn]^+$ 396 (19), $[C_{12}H_{15}N_2O_2Sn]^+$ 339 (6), $[C_8H_6N_2O_2Sn]^+$ 282 (100), $[C_8H_8N_2O_2]^+$ 164 (5), $[C_7H_6NO]^+$/$[Sn]^+$ 120 (5), $[C_4H_9]^+$ 57 (29), FT-IR (cm^{-1}, KBr): 1601s, $\nu_{C=N}$; 561m, ν_{Sn-O}; 1080m, ν_{N-N}; 478w, ν_{Sn-N};

^{1}H NMR (ppm): H-2: 6.83 (d, 1H, phenyl, $^{3}J_{H-H} = 8.4$), H-3: 7.35 (t, 1H, phenyl, $^{3}J_{H-H} = 7.8$), H-4: 6.70 (t, 1H, phenyl, $^{3}J_{H-H} = 7.2$), H-5: 7.14 (d, 1H, phenyl, $^{3}J_{H-H} = 7.8$), H-7: 8.6 [(s, 1H, CH═N), $^{3}J(^{119}Sn-^{1}H) = 38$ Hz], H-8: 7.74 (s, 1H, N═OCH), H-β: 1.33 [(s, 18H, $6CH_3$) $^{3}J(^{119/117}Sn-^{1}H) = 111, 106$ Hz]

^{13}C NMR (ppm): C-7: 162.4 (HC═N), C-8: 168.2 (CO═N), 164.0, 135.4, 134.3, 121.8, 116.6, 116.3 (Ph-C), C-α: 40.8 $^{1}J[^{119/117}Sn-^{13}C] = 586, 559$ Hz, C-β: 29.6. ^{119}Sn NMR: $\delta = -220$ Hz

*4.2.2.6. Diethyltin(IV) [N-(2-oxidobenzylidene)-N′-(oxidomethylene) hydrazine] (**6**).* Yield 80%, m.p. Viscous liquid. Anal. Calc. for $C_{12}H_{16}N_2O_2Sn$ ($M = 340$): C, 42.52; H, 4.76; N, 8.26. Found: C, 42.48; H, 4.79; N, 8.23%. EI-MS, *m/z* (%): $[C_{12}H_{16}N_2O_2Sn]^+$ 340 (64), $[C_{10}H_{11}N_2O_2Sn]^+$ 311 (100), $[C_8H_6N_2O_2Sn]^+$ 282 (75), $[C_8H_8N_2O_2]^+$ 164 (17), $[C_7H_9N_2O]^+$ 137 (10), $[C_7H_6NO]^+$/$[Sn]^+$ 120 (22), $[C_7H_5NO]^+$ 119 (24), $[C_6H_5]^+$ 77 (6), $[C_4H_9]^+$ 57 (8), FT-IR (cm^{-1}, KBr): 1602s, $\nu_{C=N}$; 577m, ν_{Sn-O}; 1077m, ν_{N-N}; 475w, ν_{Sn-N}. ^{1}H NMR (ppm): H-2: 6.78 (d, 1H, phenyl, $^{3}J_{H-H} = 8.7$), H-3: 7.35 (t, 1H, phenyl, $^{3}J_{H-H} = 7.6$), H-4: 6.70 (t, 1H, phenyl, $^{3}J_{H-H} = 7.8$), H-5: 7.15 (d, 1H, phenyl, $^{3}J_{H-H} = 7.8$), H-7: 8.62 [(s, 1H, CH═N), $^{3}J(^{119}Sn-^{1}H) = 42$ Hz], H-8: 7.67 (s, 1H, N═OCH), H-α: 1.44–1.52 (m, 4H, $2CH_2$), H-β: 1.29 (t, 6H, $2CH_3$, $^{3}J_{H-H} = 7.8$), ^{13}C NMR (ppm): C-7: 162.9 (HC═N), C-8: 167.1 (CO═N), 164.0, 135.6, 134.5, 121.7, 117.0, 116.2 (Ph-C); C-α: 14.5, $^{1}J[^{119/117}Sn-^{13}C] = 616, 589$ Hz, C-β: 9.2, $^{2}J[^{119}Sn-^{13}C] = 44$ Hz ^{119}Sn NMR: $\delta = -171$ Hz.

4.3. X-ray crystallography

X-ray diffraction data were collected on a Bruker SMART APEX CCD diffractometer, equipped with a 4K CCD detector. Data integration and global cell refinement was performed with the program *SAINT* [42]. The program suite SAINTPLUS was used for space group determination *(XPREP)* [42]. The structure was solved by Patterson method, extension of the model was accomplished by direct method and applied to different structure factors using the program *DIRDIF* [43]. Crystal data and numerical details on data collection and refinement are given in Table 1. Selected bond lengths and angles are provided in Table 2. All refinement calculations and graphics were performed with the program packages *SHELXL* [44], a locally modified version of the program *PLUTO* and *PLATON* package [45,46].

4.4. Antibacterial and antifungal activities

The antibacterial an antifungal screening were performed by using the agar well-diffusion and agar tube dilution methods, respectively [47].

4.5. Cytotoxicity

Cytotoxicity of the compounds was studies by the Brine shrimp lethality bioassay [47]. Data were analyzed with Finney's probit analysis to determine the LD_{50} [48].

4.6. Leishmanicidal activity

Leishmania major (MHOM/PK/88/DESTO) promastigotes, cultivated in bulk were aseptically sedimented down at 300 rpm, counted with the help of improved Neubaver chamber under the microscope and diluted with the fresh medium to a final concentration of 2×10^6 parasites/ml. The compounds to be checked were dissolved to a final concentration of 1.0 mg in 0.1 ml of PBS (Phosphate Buffered Saline, pH 7.4 containing 0.5% MeOH, 0.5% DMSO). In a 96-well microtiter plate, 90 ml of the parasite culture (2×10^6 parasites/ml) was added in different wells. 10 ml of the experimental compound was added in culture and serially diluted so that minimum concentration of the compound is 0.1 mg/ml 10 ml of PBS (Phosphate buffered saline, pH 7.4 containing 0.5% MeOH, 0.5% DMSO) was added as negative control while glucantime, amphotericin B, pentamidine and ampicilline to a final concentration of 1.0 mg/ml was added separately as positive control. The plate was incubated between 21 and 22 °C in dark for 5 days during which control organisms multiply 6 times. The culture was examined microscopically on an improved neubaver chamber and IC_{50} values of compounds possessing anti-leishmanial activity were calculated [49].

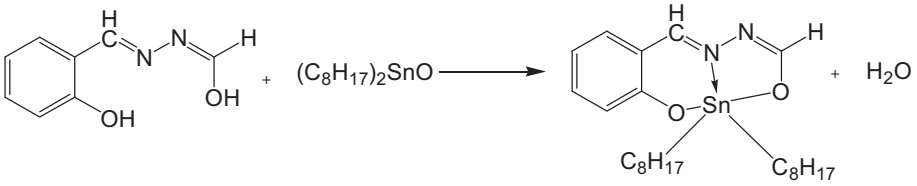

Scheme 4. Synthesis of dioctyltin(IV) derivative (**6**).

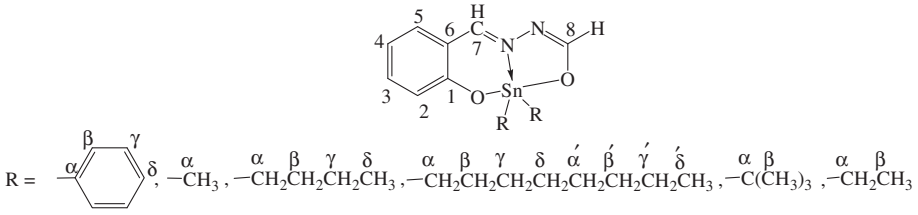

Scheme 5. Numbering scheme of organic groups and ligand.

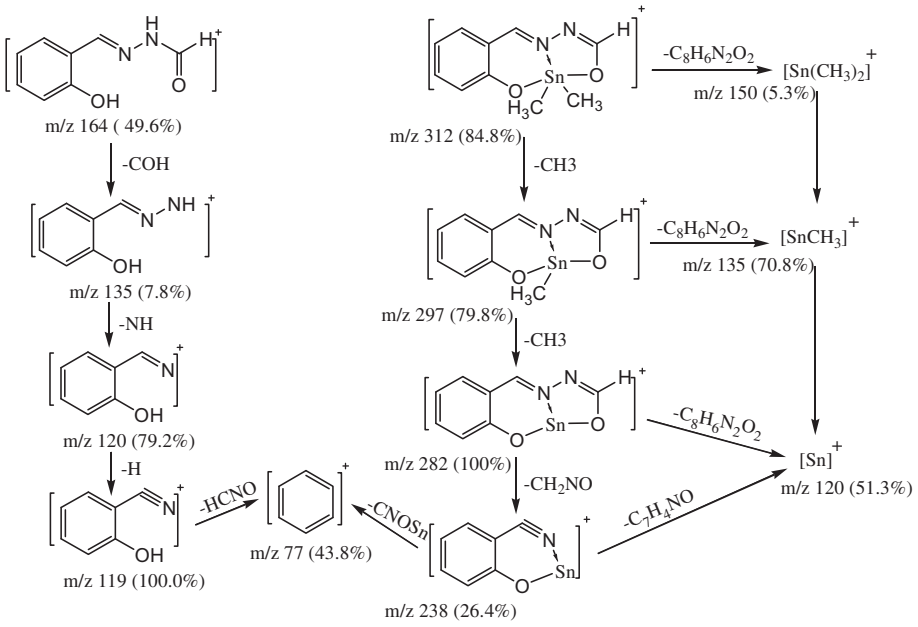

Scheme 6. Proposed mass fragmentation pattern of ligand and complex **2**.

4.7. DNA extraction

DNA was extracted from chicken blood by Falcon method [50]. The purity of DNA was checked from the ratio of absorbance at 260 and 280 nm ($A_{260}/A_{280} = 1.85$). The concentration of the DNA stock solution (2.5 mM in nucleotide phosphate, NP) was determined by monitoring the absorbance at 260 nm using the molar extinction coefficient (ε) of 6600 M^{-1} cm^{-1}.

5. Supplementary material

Crystallographic data for the structural analysis have been deposited with the Cambridge Crystallographic Data Centre, CCDC No. 698809 for Me_2SnL (**2**), Copy of this information may be obtained free of charge from the Director, CCDC, 12 Union Road, Cambridge, CBZ 1EZ, UK (fax: +44 1223 336 033; email: deposit@ccdc.cam.ac.uk or www: http://www.ccdc.cam.ac.uk).

Acknowledgements

The authors are thankful to Higher Education Commission of Pakistan for financial support.

References

[1] S. Tabassum, C. Pettinari, J. Organomet. Chem. 691 (2006) 1761–1766.
[2] M. Gielen, M. Biesemans, R. Willem, Appl. Organomet. Chem. 19 (2005) 440–450.
[3] P. Yang, M. Guo, Coord. Chem. Rev. 185 (1999) 189–211.
[4] A.J. Crowe, Antitumor activity of tin compounds. in: S.P. Fricker (Ed.), Metal Compounds in Cancer Therapy. Chapman & Hall, London, 1994, p. 147.
[5] T.B. Baul, C. Masharing, G. Ruisi, R. Jirasko, M. Holcapek, D. de Vos, D. Wolstenholme, A. Linden, J. Organomet. Chem. 692 (2007) 4849–4862.
[6] H.D. Yin, S.W. Chen, L.W. Li, D.Q. Wang, Inorg. Chim. Acta 360 (2007) 2215–2223.
[7] H.D. Yin, M. Hong, G. Li, D.Q. Wang, J. Organomet. Chem. 690 (2005) 3714–3719.
[8] M. Cagnoli, A. Alama, F. Barbieri, F. Novelli, C. Bruzzo, F. Sparatore, Anticancer Drugs 9 (1998) 603–610.
[9] X. Song, A. Zapata, G. Eng, J. Organomet. Chem. 691 (2006) 1756–1760.
[10] D.K. Dey, A. Lycka, S. Mitra, G.M. Rosair, J. Organomet. Chem. 689 (2004) 88–95.
[11] M. Gielen, Appl. Organomet. Chem. 16 (2002) 481–494.
[12] H. Yin, J. Cui, Y. Qiao, Polyhedron 27 (2008) 2157–2166.
[13] M.A. Ali, A.H. Mirzam, A.L. Tan, L.K. Wei, P.V. Bernhardt, Polyhedron 23 (2004) 2037–2043.
[14] C. Pettinari, F. Marchetti, R. Pettinari, D. Martini, A. Drozodov, S. Troyanov, Inorg. Chim. Acta 325 (2001) 103–114.
[15] T.P. Lockhart, W.F. Manders, Inorg. Chem. 25 (1986) 892–895.
[16] T.P. Lockhart, F. Davidson, Organometallics 6 (1987) 2471–2478.
[17] M. Nádvorník, J. Holeček, K. Handlíř, A. Lyčka, J. Organomet. Chem. 275 (1984) 43–51.
[18] S. Shuja, S. Ali, S.A. Meetsma, G.A. Broker, E.R.T. Tiekink, Acta Crystallogr. E63 (2007) m1130–m1132.
[19] A.W. Addison, T.N. Rao, J. Reedijk, J. van Rijn, G.C. Verschoor, J. Chem. Soc., Dalton Trans. 7 (1984) 1349–1356.
[20] L. Shi, H.M. Ge, S.H. Tan, H.Q. Li, Y.C. Song, H.L. Zhu, R.X. Tan, Eur. J. Med. Chem. 42 (2007) 558–564.
[21] P. Panneerselvam, R.R. Nair, G. Vijayalakshmi, E.H. Subramanian, S.K. Sridhar, Eur. J. Med. Chem. 40 (2005) 225–229.
[22] J. Mann, M.J.C. Crabbe, Bacteria and Antibacterial Agents. Spectrum Academic Publishers, Oxford, UK, 1990, pp. 74.
[23] P. Mushak, M. Krigman, R.B. Mailman, Neurobehav. Toxicol. Teratol. 4 (1982) 209–215.

[24] S.V. Doctor, D.A. Fox, Toxicol. Environ. Health 10 (1982) 53–62.
[25] A.V. Krishnaraju, T.V.N. Rao, D. Sundararaju, M. Vanisree, H.S. Tsay, G.V. Subbaraju, Int. J. Appl. Sci. Eng. 4 (2006) 115–125.
[26] S. Shahzadi, K. Shahid, S. Ali, M. Bakhtiar, Turk. J. Chem. 32 (2008) 333–353.
[27] M. Aslanoglu, Anal. Sci. 22 (2006) 439–443.
[28] E.C. Long, J.K. Barton, Acc. Chem. Res. 23 (1990) 271–273.
[29] Q. Feng, N.Q. Li, Y.Y. Jiang, Anal. Chim. Acta 344 (1997) 97–104.
[30] R. Vijayalakshmi, M. Kanthimathi, R. Parthasarathi, B.U. Nair, Bull. Chem. Soc. Jpn. 78 (2005) 270–276.
[31] Q. Lie, P. Yang, H. Wang, M. Guo, J. Inorg. Biochem. 64 (1996) 181–195.
[32] J. Rusanova, S. Decurtins, E. Rosanov, H.S. Evans, S. Delahaye, A. Hauser, J. Chem. Soc., Dalton Trans. (2002) 4318–4320.
[33] A. Ambroise, B.G. Maiya, Inorg. Chem. 39 (2000) 4264–4272.
[34] J.E.B. Randles, Trans. Faraday Soc. 44 (1948) 327–338.
[35] A. Sevcik, Collect. Czech. Chem. Commun. 13 (1948) 337–349.
[36] S. Wang, T. Penz, C.F. Yang, Biophys. Chem. 104 (2003) 239–248.
[37] X. Yang, G.L. Shen, R.Q. Yu, Microchem. J. 62 (1999) 394–404.
[38] Z. Xu, G. Bai, C. Dong, Bioorg. Med. Chem. 13 (2005) 5694–5699.
[39] M.Y. Ni, Y. Wang, H.L. Li, Pol. J. Chem. 71 (1997) 816–822.
[40] M.S. Ibrahim, I.S. Shehatta, A.A. Al-nyeli, J. Pharm. Biomed. Anal. 28 (2002) 217–225.
[41] D.D. Perrin, W.L.F. Armengo, Purification of Laboratory Chemicals, third ed. Pergamon Press, Oxford, 1988.
[42] Bruker, Smart, SAINTPLUS and XPREP. Area Detector Control and Integration Software. Smart Apex Software Reference Manuals. Bruker Analytical X-ray Instruments. Inc, Madison, Wisconsin, USA, 2006.
[43] P.T. Beurskens, G. Beurskens, R. Gelder, S. García-Granda, S.R.O. Gould, R. Israël, J.M.M. Smits, The DIRDIF-99 Program System, Crystallography Laboratory. University of Nijmegen, The Netherlands, 1999.
[44] G.M. Sheldrick, SHELXL-97. Program for the Refinement of Crystal Structures. University of Göttingen, Germany, 1997.
[45] A. Meetsma, PLUTO. Molecular Graphics Program. 2007. University of Groningen, The Netherlands, 2006.
[46] A.L. Spek, PLATON. Program for the Automated Analysis of Molecular Geometry. University of Utrecht, The Netherlands, 2006.
[47] A. Rahman, M.I. Choudhary, W.J. Thomsen, Bioassay Techniques for Drug Development. Harward Academic Press, Amsterdam, 2001.
[48] D.J. Finney, Probit Analysis, third ed. Cambridge University Press, Cambridge, 1971.
[49] K.M. Khan, M. Rasheed, Z. Ullah, S. Hayat, F. Kaukab, M.I. Choudhary, A. Rahman, S. Perveen, Bioorg. Med. Chem. 11 (2003) 1381–1387.
[50] J. Sambrook, E.F. Fritsch, T. Maniatis, Molecular Cloning: a Laboratory Manual, second ed. Cod. Spring harbour laboratory press, New York, 1989.